

# Throat effects on shadows of Kerr-like wormholes

Shinta Kasuya and Masataka Kobayashi

*Department of Mathematics and Physics, Kanagawa University, Kanagawa 259-1293, Japan*

(Dated: March 24, 2021)

We revisit to investigate shadows cast by Kerr-like wormholes. The boundary of the shadow is determined by unstable circular photon orbits. We find that, in certain parameter regions, the orbit is located at the throat of the Kerr-like wormhole, which was not considered in the literatures. In these cases, the existence of the throat alters the shape of the shadow significantly, and it will be much easier to differentiate it from that of a Kerr black hole.

## I. INTRODUCTION

A wormhole is a spacetime bridge connecting two separate points in spacetime [1–4]. (For early review, see [5], for example.) Astrophysically, it is plausible to regard that wormholes are rotating. One of the metric for the rotating wormhole is the Kerr-like wormhole proposed in Ref. [6]. It is important to distinguish this wormhole from the Kerr black hole, and one such way is to study shadows of the Kerr-like wormholes [7]. Remarkable attention to shadows cast by compact objects grows recently, since the Event Horizon Telescope observed the black hole shadow at the center of the galaxy M87 [8].

In this article, we revisit to investigate shadows of the Kerr-like wormhole. The shadow boundary can be estimated by considering unstable circular photon orbits. In Ref. [7], it was found that the size of the shadow is smaller than that of the Kerr black hole for the same mass, with two shapes being similar figures. We point out that the effects of the wormhole throat become prominent when the unstable circular photon orbits are located at the throat in certain parameter space. In these cases, the shape of the shadow is altered considerably, and it will be much easier for us to figure out the differences. In the study of the shadows of other types of the rotating wormholes [9], similar results were obtained in Ref. [10], where the throat effects on the shadows were taken into account.

The structure of the article is as follows. In the next section, we introduce the metric of the Kerr-like wormhole, and show some of its features. In Sec. III, we derive unstable circular photon orbits from the radial geodesic equation, where we recollect the results in Ref. [7] in Sec. III A, and point out that the unstable circular photon orbit can lie at the throat in some parameter regions in Sec. III B. We show the shapes of the shadows on the celestial plane with and without the effects of the throat in Sec. IV. Sec. V is devoted to our conclusions.

## II. KERR-LIKE WORMHOLE

The metric of the Kerr-like wormhole was constructed with slight modification from the metric of the Kerr black hole, which reads, in Boyer-Lindquist coordinates, as [6,

7]

$$ds^2 = - \left( 1 - \frac{2Mr}{\Sigma} \right) dt^2 - \frac{4Mar \sin^2 \theta}{\Sigma} dt d\phi + \frac{\Sigma}{\Delta} dr^2 + \Sigma d\theta^2 + \left( r^2 + a^2 + \frac{2Ma^2 r \sin^2 \theta}{\Sigma} \right) \sin^2 \theta d\phi^2, \quad (1)$$

where

$$\Sigma = r^2 + a^2 \cos^2 \theta, \quad (2)$$

$$\Delta = r^2 + a^2 - 2M(1 + \lambda^2)r. \quad (3)$$

Here  $\lambda$  represents the deviation parameter such that the metric reduces to that of the Kerr black hole for  $\lambda = 0$ .  $M$  and  $aM$  respectively denote the mass and the angular momentum of the would-be Kerr black hole. This metric is a rotational version of the Schwarzschild-like wormhole proposed in Ref. [11], which is recovered by setting  $a = 0$ .

Instead of having an event horizon, the Kerr-like wormhole spacetime has a throat. It is evaluated by  $\hat{\Delta}(r_{\text{throat}}) = 0$ , so that we obtain the throat radius as [6]

$$r_{\text{throat}} = M(1 + \lambda^2) + \sqrt{M^2(1 + \lambda^2)^2 - a^2}. \quad (4)$$

The ADM mass of the Kerr-like wormhole is estimated as [7]

$$M_{\text{WH}} = M(1 + \lambda^2), \quad (5)$$

as seen by an observer at the asymptotic spatial infinity.

## III. UNSTABLE CIRCULAR PHOTON ORBITS

Null geodesic equations govern the trajectory of light. For stationary and axisymmetric spacetime, it is characterized by three constants: the photon energy  $E$ , angular momentum  $L$ , and the Carter constant  $\mathcal{K}$  [12]. Four null

geodesic equations are obtained as [6, 7]

$$\Sigma \frac{dt}{d\sigma} = -a(aE \sin^2 \theta - L) + \frac{(r^2 + a^2)\mathcal{P}}{\Delta}, \quad (6)$$

$$\Sigma \frac{d\phi}{d\sigma} = -\left(aE - \frac{L}{\sin^2 \theta}\right) + \frac{a\mathcal{P}}{\Delta}, \quad (7)$$

$$\Sigma \frac{dr}{d\sigma} = \pm \sqrt{\mathcal{R}}, \quad (8)$$

$$\Sigma \frac{d\theta}{d\sigma} = \pm \sqrt{\Theta}, \quad (9)$$

where  $\sigma$  is the affine parameter, and

$$\Delta = r^2 + a^2 - 2Mr, \quad (10)$$

$$\mathcal{P} = (r^2 + a^2)E - aL, \quad (11)$$

$$\mathcal{R} = \frac{\hat{\Delta}}{\Delta} \left\{ \mathcal{P}^2 - \Delta [\mathcal{K} + (L - aE)^2] \right\}, \quad (12)$$

$$\Theta = \mathcal{K} + \cos^2 \theta \left( a^2 E^2 - \frac{L^2}{\sin^2 \theta} \right). \quad (13)$$

We consider a wormhole connecting two regions of the spacetime, where light sources illuminate around the wormhole in one region, and there is none in the vicinity of the wormhole in the other region. In the former region, the light propagation can be divided into two categories. The first one is that the light plunges into the wormhole passing its throat away to the other region, and the second one is that the light is scattered away to the infinity in the same region. The distant observer in this region sees the bright and dark zones whose boundary is determined by that of the two categories. This dark zone is referred to as the shadow of the wormhole.

In order to find the shadow, therefore, we need to specify that boundary, which is represented by the unstable circular photon orbits around the wormhole. To this end, we rewrite the radial geodesic equation (8) as

$$\frac{1}{2} \left( \frac{dr}{d\sigma} \right)^2 + V_{\text{eff}} = 0. \quad (14)$$

Here  $V_{\text{eff}}(r)$  can be regarded as the effective potential, given by

$$V_{\text{eff}} = -\frac{1}{2\Sigma^2} \mathcal{R} = -\frac{E^2}{2} \frac{\hat{\Delta}(r)X(r)}{Y(r)} \equiv -\frac{E^2}{2} \tilde{V}_{\text{eff}}, \quad (15)$$

where we use the impact parameters  $\xi = L/E$  and  $\eta = \mathcal{K}/E^2$ , and

$$X(r) = (r^2 + a^2 - a\xi)^2 - \Delta(r) [\eta + (\xi - a)^2], \quad (16)$$

$$Y(r) = \Sigma^2(r)\Delta(r). \quad (17)$$

The radius of the unstable circular photon orbit  $r_{\text{ph}}$  is derived by the conditions:

$$V_{\text{eff}}(r_{\text{ph}}) = 0, \quad V'_{\text{eff}}(r_{\text{ph}}) = 0, \quad V''_{\text{eff}}(r_{\text{ph}}) < 0, \quad (18)$$

where the prime denotes the derivative with respect to  $r$ , which leads to the conditions in terms of  $\tilde{V}_{\text{eff}}$  as

$$\tilde{V}_{\text{eff}}(r_{\text{ph}}) = 0, \quad \tilde{V}'_{\text{eff}}(r_{\text{ph}}) = 0, \quad \tilde{V}''_{\text{eff}}(r_{\text{ph}}) > 0. \quad (19)$$

Since  $Y(r) \neq 0$  for  $r > r_{\text{throat}}$ , the first condition is satisfied for (i)  $X(r_{\text{ph}}) = 0$ , or (ii)  $\hat{\Delta}(r_{\text{ph}}) = 0$ . The case (i) was investigated in Ref. [7], but the case (ii) was overlooked. We will come back to the case (ii) in Sec. III B, and keep considering only the case (i) in the following subsection.

#### A. The case (i) $X(r_{\text{ph}}) = 0$

In this case, the second and third conditions read as  $X'(r_{\text{ph}}) = 0$  and  $X''(r_{\text{ph}}) > 0$ , respectively. Then, from the first and second conditions, the impact parameters can be given in terms of  $r_{\text{ph}}$  as [7]

$$\xi = \frac{r_{\text{ph}}^2(r_{\text{ph}} - 3M) + a^2(r_{\text{ph}} + M)}{a(M - r_{\text{ph}})}, \quad (20)$$

$$\eta = \frac{4a^2 M r_{\text{ph}}^3 - r_{\text{ph}}^4 (r_{\text{ph}} - 3M)^2}{a^2(M - r_{\text{ph}})^2}.$$

The range of the radius of the unstable circular photon orbit  $r_{\text{ph}}$  is estimated as

$$r_{\text{ph}}^{(\min)} < r_{\text{ph}} < r_{\text{ph}}^{(\max)}, \quad (21)$$

where

$$r_{\text{ph}}^{(\min/\max)} = 2M \left\{ 1 + \cos \left[ \frac{2}{3} \cos^{-1} \left( (-/+)\frac{a}{M} \right) \right] \right\}, \quad (22)$$

which correspond to the prograde/retrograde orbits on the equatorial plane, respectively [13]. Of course, they are roots of the equation  $\eta(r) = 0$ .

From the third condition,  $X''(r_{\text{ph}}) > 0$ ,  $r_{\text{ph}}$  must obey  $r_{\text{ph}} > r_{3\text{rd}}$ , where  $r_{3\text{rd}}(>0)$  is a root of

$$r^3 - 3Mr^2 + 3M^2r - Ma^2 = 0. \quad (23)$$

Since one can easily see that  $r_{3\text{rd}} < M$ , we always have  $r_{\text{ph}} > r_{3\text{rd}}$ .

The non-rotating case ( $a = 0$ ) should be considered separately. In this case, we obtain the fixed unstable circular orbit and the relation between two impact parameters respectively as

$$r_{\text{ph}} = 3M, \quad \eta = 27M^2 - \xi^2. \quad (24)$$

As for the third condition in Eq.(19),  $\eta$  and  $\xi$  must satisfy the constraint

$$\eta < 54M^2 - \xi^2, \quad (25)$$

where we use  $r_{\text{ph}} = 3M$ . Here this condition is always accomplished.

A note follows as in Ref. [7]. The expression of the unstable circular photon orbits, (20) with (21), or (24), are exactly the same as those for the Kerr black hole whose metric is given by Eq.(1) with  $\lambda = 0$ . In the Kerr-like wormhole case, however, it is the ADM mass (5) that is seen by the observer, so that  $M$  scales as  $M_{\text{WH}}/(1 + \lambda^2)$ . On the other hand, the ADM mass of the Kerr black hole reads as  $M_{\text{BH}} = M$ . Therefore, the radius of the unstable circular photon orbits is smaller for the Kerr-like wormhole than that of the Kerr black hole with the same mass.

### B. The case (ii) $\hat{\Delta}(r_{\text{ph}}) = 0$

As mentioned above, it was overlooked in Ref. [7] that the radius of the unstable circular photon orbit given in Eqs.(20) with (21), or (24), would be smaller than the throat radius  $r_{\text{throat}}$  for some parameter ranges. This is the case that the unstable circular photon orbit is located at the throat:

$$r_{\text{ph}} = r_{\text{throat}}. \quad (26)$$

The throat effect starts to appear when  $r_{\text{throat}}$  becomes larger than  $r_{\text{ph}}^{(\min)}$ , and completely dominates for  $r_{\text{throat}} > r_{\text{ph}}^{(\max)}$ . These regions are depicted in Fig. 1. Red and blue lines represent  $r_{\text{throat}} = r_{\text{ph}}^{(\min)}$  and  $r_{\text{throat}} = r_{\text{ph}}^{(\max)}$ , respectively. The throat affects the shadow partially for the parameters above the red line, and determines the shadow completely for those above the blue line.

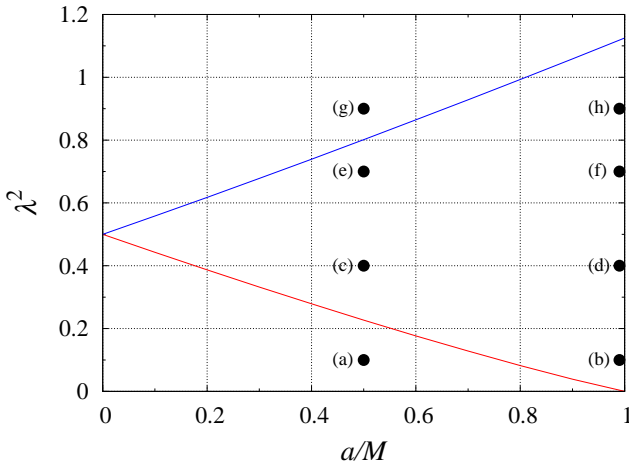


FIG. 1: Regions where the throat affects the shape of shadow in parameter space  $(a/M, \lambda^2)$ . Red and blue lines denote  $r_{\text{throat}} = r_{\text{ph}}^{(\min)}$  and  $r_{\text{throat}} = r_{\text{ph}}^{(\max)}$ , respectively. Unstable circular photon orbits (20) or (24) control the shadow shapes below the red line, while the throat solely determines them above the blue line. In between, both effects form the shapes of the shadow. Dots (a) - (h) indicate the parameters used in Fig. 3.

In this case, using, in addition, the second condition in Eq.(19), which leads to  $X(r_{\text{ph}}) = 0$ , we obtain the relation between  $\eta$  and  $\xi$  as

$$\begin{aligned} \eta &= \frac{(r_{\text{throat}}^2 + a^2 - a\xi)^2}{\Delta(r_{\text{throat}})} - (\xi - a)^2 \\ &= \frac{[2M(1 + \lambda^2)r_{\text{throat}} - a\xi]^2}{2M\lambda^2 r_{\text{throat}}} - (\xi - a)^2, \end{aligned} \quad (27)$$

where we use Eqs.(3) and (10) in the last line.

The third condition in Eq.(19) is reduced to  $X'(r_{\text{ph}}) > 0$ . This leads to

$$\eta < \frac{2r_{\text{throat}}}{r_{\text{throat}} - M} [2M(1 + \lambda^2)r_{\text{throat}} - a\xi] - (\xi - a)^2. \quad (28)$$

## IV. SHADOWS

The observer sees the projection of the unstable circular orbits, (20) with (21), (24), or (27), as the boundary of the wormhole shadow at the so-called observer's sky, the plane passing through the wormhole and normal to the line of sight of the observer. The celestial coordinates  $\alpha$  and  $\beta$  measure the positions on this plane, and they can be written as [14]

$$\begin{aligned} \alpha &= \lim_{r_{\text{obs}} \rightarrow \infty} \left( -r^2 \sin \theta_0 \frac{d\phi}{dr} \right)_{\text{obs}}, \\ \beta &= \lim_{r_{\text{obs}} \rightarrow \infty} \left( r^2 \frac{d\theta}{dr} \right)_{\text{obs}}, \end{aligned} \quad (29)$$

where  $\theta_0$  denotes the inclination angle between the rotation axis of the wormhole and the line of sight, and the subscripts “obs” represent the values evaluated at the observer's position. Using the geodesic equations (7) - (9), we have [7]

$$\begin{aligned} \alpha &= -\frac{\xi}{\sin \theta_0} = -\xi, \\ \beta &= \pm \sqrt{\eta + a^2 \cos^2 \theta_0 - \frac{\xi^2}{\tan^2 \theta_0}} = \pm \sqrt{\eta}, \end{aligned} \quad (30)$$

where the last equalities are estimated when the observer is located on the equatorial plane ( $\theta_0 = 90^\circ$ ).

It is instructive to show the non-rotating case ( $a = 0$ ) in the first place. In this case,  $r_{\text{ph}} = 3M$  for  $\lambda^2 \leq \frac{1}{2}$ , while  $r_{\text{ph}} = r_{\text{throat}} = 2M(1 + \lambda^2)$  for  $\lambda^2 > \frac{1}{2}$ , and the shadow exhibits just a circle on the celestial plane as

$$\alpha^2 + \beta^2 = \begin{cases} 27M^2, & (\lambda^2 \leq \frac{1}{2}), \\ \frac{4(1 + \lambda^2)^3}{\lambda^2} M^2, & (\lambda^2 > \frac{1}{2}). \end{cases} \quad (31)$$

As mentioned, since the observer sees the wormhole mass  $M_{\text{WM}} = M(1 + \lambda^2)$ , we normalize the parameters

with respect to  $M_{\text{WH}}$ , which implies that we set  $M_{\text{WH}} = 1$ . Then the shadow radius  $R$  on the celestial plane is written as

$$R^2 = \begin{cases} \frac{27}{(1 + \lambda^2)^2}, & (\lambda^2 \leq \frac{1}{2}), \\ \frac{4(1 + \lambda^2)}{\lambda^2}, & (\lambda^2 > \frac{1}{2}), \end{cases} \quad (32)$$

displayed in Fig. 2. Red and blue lines denote the cases for  $\lambda^2 > \frac{1}{2}$  and  $\lambda^2 \leq \frac{1}{2}$ , respectively. The solid lines show the radius of the shadow. Therefore, the actual size of the shadow becomes larger for  $\lambda^2 > \frac{1}{2}$ , which is the impact of the throat.

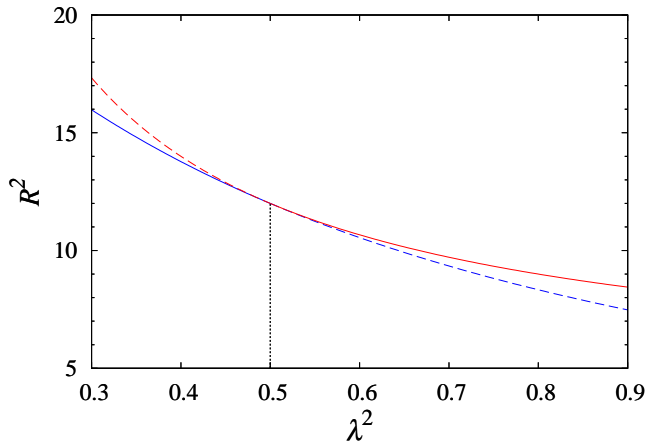


FIG. 2: Radius of the shadow on the celestial plane for  $a = 0$ , shown in Eq.(32). Red and blue lines represent respectively the cases with and without the effects of the throat. Solid lines express the actual sizes of the shadows.

Notice that  $\lambda = 0$  reduces to the non-rotating black hole case whose shadow radius is estimated as  $R^2 = 27$  for  $M_{\text{BH}} = 1$ .

The third condition in Eq.(19) is rewritten in terms of  $R$  as

$$R^2 < \begin{cases} \frac{54}{(1 + \lambda^2)^2}, & (\lambda^2 \leq \frac{1}{2}), \\ \frac{16(1 + \lambda^2)}{1 + 2\lambda^2}, & (\lambda^2 > \frac{1}{2}), \end{cases} \quad (33)$$

where Eqs.(25) and (28) are used. Therefore,  $R^2$  in Eq.(32) always meets this condition.

Now let us move on to the general situations when the wormhole is rotating ( $a \neq 0$ ). We consider the case when the observer is on the equatorial plane ( $\theta_0 = 90^\circ$ ), since it is the most apparent situation to see the effect of rotation.

In order to find the shape of the shadow, we should insert the impact parameters (20) into the celestial coordinate (30), and vary the unstable circular photon radius  $r_{\text{ph}}$  in the range (21). This is the case which the

throat has nothing to do with, and was investigated in Ref. [7]. We show the shadow in the case with  $a = 0.5$  and  $\lambda^2 = 0.1$  in solid blue line in Fig. 3(a) as an example. Also shown in dashed blue line is the shadow of the Kerr black hole with the same angular momentum and the same mass as the Kerr-like wormhole, so that we set  $M_{\text{BH}} = M_{\text{WH}} = 1$ . Note that the shapes of two shadows are similar figures.

The effects of the throat on the shadow appears for larger  $a$ , which was overlooked in Ref. [7]. We show an example case with  $a = 0.99$  and  $\lambda^2 = 0.1$  in Fig. 3(b). Here again the shadow of the wormhole without throat effects is displayed by a solid blue line, while we denote the shadow of the black hole in a dashed blue line.

Red line comes newly from the effects of the wormhole throat considered in Sec. III B. Here, we put the impact parameters in Eq.(27) into celestial coordinates (30) to find the boundary on the celestial plane. Therefore, the shape of the wormhole shadow does not shrink too much for the prograde orbits because of the existence of the wormhole throat. As a result, while the shapes of solid and dashed blue lines are similar figures, the red line deforms the shape of the wormhole shadow so that we can distinguish between the shadows of a wormhole and a black hole more easily.

The effects of the throat becomes more remarkable in larger  $\lambda$  cases. We show these cases in Fig. 3(c)-(f) and (h), where the throat effects deform the shapes of the shadows to certain extents. In these cases, the radius of the throat  $r_{\text{throat}}$  is larger than the prograde radius  $r_{\text{ph}}^{(\text{min})}$ , but smaller than the retrograde radius  $r_{\text{ph}}^{(\text{max})}$ .

Finally, the whole shadow shape is determined by the throat, for example, in the case with  $a = 0.5$  and  $\lambda^2 = 0.9$ , shown in Fig. 3(g). In this situation, the shadow shape of the wormhole in red line is completely different from that of the black hole in dashed blue line. Note that the shape differs also from a circle. See Eq.(27).

Note that the third condition in Eq.(19) is satisfied in all the cases. Therefore, the obtained circular photon orbits are indeed unstable.

## V. CONCLUSIONS

We have revisited to investigate the shadow cast by the Kerr-like wormhole. The boundary of the shadow is determined by unstable circular photon orbits. We have found that, in certain parameter regions, the orbit is located at the throat of the Kerr-like wormhole, which was not considered in the literatures. These cases take place for larger wormhole spin  $a$  and/or larger deviation parameter  $\lambda$ . The existence of the throat alters the shape of the shadow considerably, and it will be much easier to differentiate it from that of the Kerr black hole, compared with those cases without the throat effects taken into account, where the shapes of the Kerr-like wormhole and the Kerr black hole are found to be similar figures.

On the other hand, we can get another perspectives.

If there are throat effects on the shadow shape, one can figure out whether the observed shadow is cast by the Kerr-like wormhole or the Kerr black hole even in the

case when the object mass is unknown, not determined by other observations such as by motions of objects around the wormhole/black hole.

- 
- [1] L. Flamm, *Physik. Z.* **17**, 448-454 (1916).
  - [2] A. Einstein and N. Rosen, *Phys. Rev.* **48**, 73-77 (1935).
  - [3] H. G. Ellis, *J. Math. Phys.* **14**, 104-118 (1973).
  - [4] M. S. Morris and K. S. Thorne, *Am. J. Phys.* **56**, 395-412 (1988).
  - [5] M. Visser, *Lorentzian wormholes: From Einstein to Hawking* (AIP Press, 1995).
  - [6] P. Bueno, P. A. Cano, F. Goelen, T. Hertog and B. Vernocke, *Phys. Rev. D* **97**, no.2, 024040 (2018).
  - [7] M. Amir, K. Jusufi, A. Banerjee and S. Hansraj, *Class. Quant. Grav.* **36**, no.21, 215007 (2019).
  - [8] K. Akiyama *et al.* [Event Horizon Telescope], *Astrophys. J. Lett.* **875**, L1 (2019).
  - [9] P. G. Nedkova, V. K. Tinchev and S. S. Yazadjiev, *Phys. Rev. D* **88**, no.12, 124019 (2013).
  - [10] R. Shaikh, *Phys. Rev. D* **98**, no.2, 024044 (2018); G. Gylulchev, P. Nedkova, V. Tinchev and S. Yazadjiev, *Eur. Phys. J. C* **78**, no.7, 544 (2018).
  - [11] T. Damour and S. N. Solodukhin, *Phys. Rev. D* **76**, 024016 (2007).
  - [12] B. Carter, *Phys. Rev.* **174**, 1559-1571 (1968).
  - [13] J. M. Bardeen, W. H. Press and S. A. Teukolsky, *Astrophys. J.* **178**, 347 (1972).
  - [14] I. Bray, *Phys. Rev. D* **34**, 367 (1986); S. E. Vazquez and E. P. Esteban, *Nuovo Cim. B* **119**, 489-519 (2004).

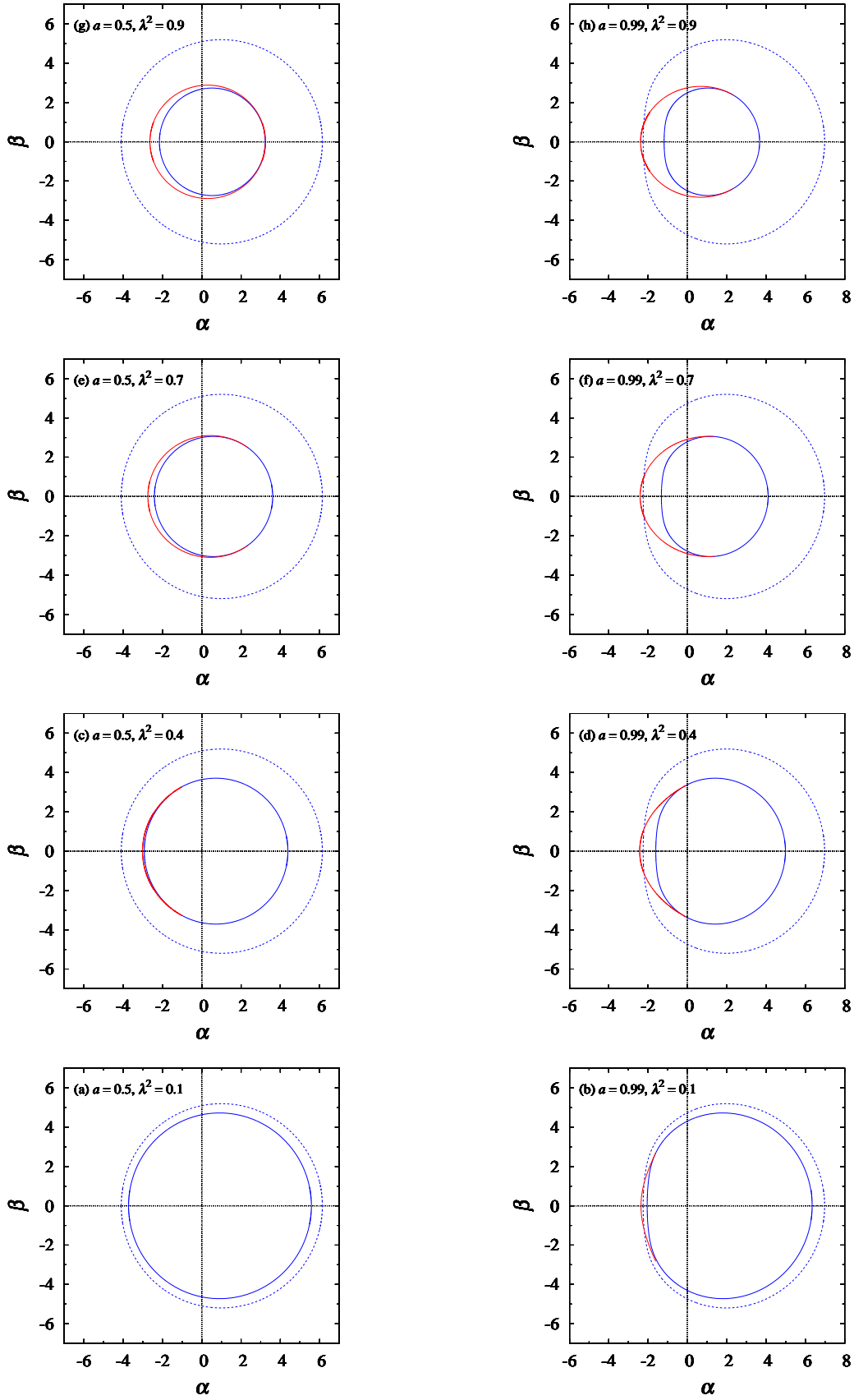


FIG. 3: Shadows of the Kerr-like wormholes on the celestial plane for  $a = 0.5$  in the left row and  $a = 0.99$  in the right row with  $\lambda^2 = 0.1, 0.4, 0.7$ , and  $0.9$  from the bottom to the top, respectively. (a) - (h) cases correspond to the parameters marked with dots in Fig. 1.